International Core Journal of Engineering Volume 10 Issue 1, 2024
ISSN: 2414-1895 DOI: 10.6919/ICJE.202401_10(1).0005

Evaluation of Tensile Characteristics of Plastic Geogrid Considering the Effect of Side Restraint

Biao Li[1, a], Qiaoyi Li[2, *], Lina Cao[2, b], Wensi Pei[2, c], Wenhao Han[2, d]

[1] Shijiazhuang Transportation Investment & Development Co., Ltd, Shijiazhuang, 050030, Hebei, China

[2] Hebei GEO University, Shijiazhuang, 050031, Hebei, China

[a]yanglb@stdu.edu.cn, [*]liqiaoyi@stdu.edu.cn, [b]linacao2023@163.com, [c]pws09048@163.com, [d]18812151913@163.om

Abstract

The multi-rib tensile test is often used on the geogrid reinforcement of embankment slopes. However, the existing tensile test method reflects the practical engineering and only considers the tensile characteristics of the geogrid laid in the width direction, and neglects the limiting effect of the length direction on the tensile strain in the width direction. In this paper, the tensile characteristics of geogrids with side restraint are studied by using an in-house designed tensile test device. The results show that the peak strain decreases and the tensile yield strength increases in comparison to values without side restraint. The tensile extension rate had little effect on the difference in tensile yield strength between with and without side restraint. The difference in peak strain between with and without side restraint decreased with the increase of tensile extension rate. The secant stiffness improvement factors of geogrid at 5% were observed to be close to 1 at the four different tensile extension rates. With the extension rate increase, the failure mode changed from ductile fracture to brittle fracture.

Keywords

Geogrid; Tensile Characteristic; Side Restraint; Peak Strain; Tensile Yield Strength; Secant Stiffness Improvement Factor; Failure Mode.

1. Introduction

Biaxial plastic geogrid plays an important role in improving bearing capacity and regulating uneven settlement in composite pile-reinforced foundation with cushion.[1] In a reinforced embankment slope, it mainly plays the role of improving the subgrade durability, preventing sliding of the slope shallow layer, and controlling the subgrade layer filling and compaction quality.[2–5] As a polymeric material, the tensile strength and strain characteristics of a plastic geogrid are affected, not only by the production process but also by the soil medium environment and the tensile extension rate in engineering application.

Hegazy R and Yang Guangqing [6,7] carried out tensile tests on geogrids at different rates, and pointed out that the extension rate has great influence on their mechanical properties. Lin Yuliang et al. [8] determined that the mechanical behavior of large diameter grids and high strength geogrids is better than that of small diameter grids and low strength geogrids through tensile tests on grids and geogrids. McGown et al. [9] discussed the ‘static interlock’ concept, where particles in the soil smaller than the geogrid openings penetrate through the openings. Zhang Mengxi et al. [10] studied the dynamic strain and cyclic softening characteristics of geogrids by a cyclic tensile test. Wang Enliang et al. [11] showed that the tensile strength of plastic geogrid is significantly improved at low

ISSN: 2414-1895 DOI: 10.6919/ICJE.202401_10(1).0005

temperature. S. Balakrishnan [12] studied the tensile stress-strain characteristics of geogrids in soil, indicating that soil can effectively increase the geogrid stiffness.

The multi-rib tensile test [13] is often used to determine the tensile load-strain characteristics of plastic geogrids. However, the multi-rib tensile test method reflects the practical engineering and only considers the tensile characteristics of the geogrid laid in the width direction, and neglects the limiting effect of the length direction on the tensile strain in the width direction. In order to explore the influence of side restraint on the tensile characteristic of biaxial plastic geogrids, an in-house designed tensile test device was used to conduct laboratory side restrained tensile tests on geogrids to evaluate their tensile behavior. The influence of side restraint at different tensile extension rates on plastic geogrid behaviour was researched. The changes of peak strain and secant modulus were analyzed. The research results can provide a reference for the engineering application of geogrids and design of reinforced soil structures.

2. Tensile Deformation Mechanism of Biaxial Geogrid

2.1 Production Process of Biaxial Plastic Geogrid

Biaxial tensile geogrid is made from high-quality polypropylene plate with uniform thickness and a smooth surface. Then, the plate is punched and stretched in the longitudinal and transverse directions by machine in a preheated environment. In the whole stretching process, the longitudinal and transverse connecting parts surrounding the holes are stretched into ribs. The molecules in the ribs are highly oriented along the stretching direction, the ribs become thinner and the tensile properties of the material are improved. The longitudinal and transverse joints around the hole are nodes, and the joint thickness remains basically the same as the plate thickness.

2.2 The Microstructure Analysis of Biaxial Plastic Geogrid

Considering the structure of a crystalline polymer, the biaxial geogrid can be divided into three zones (Fig. 1).

I, tensile zone, the rib part in which the molecular chain has been stretched and which is in an oriented ellipsoid crystalline state;

III, the non-oriented spherulitically structured zone, the node part without stretching;

II, transition zone, the connecting part between rib and node; in this zone, the structural state is relatively complex. There are not only spherulitic structures without orientation, but also ellipsoidal crystalline structure. Crystalline polymers have different structural morphologies before and after orientation by stretching.

Through stretching oriented crystallization, the structure of the polymer is fibrous and has obvious anisotropic characteristics. Without oriented crystallization, the structure of the polymer is spherulitic or stacked lamellar. Fig. 2 shows the result of scanning electron microscope pictures of each part of a biaxial tensile plastic geogrid.

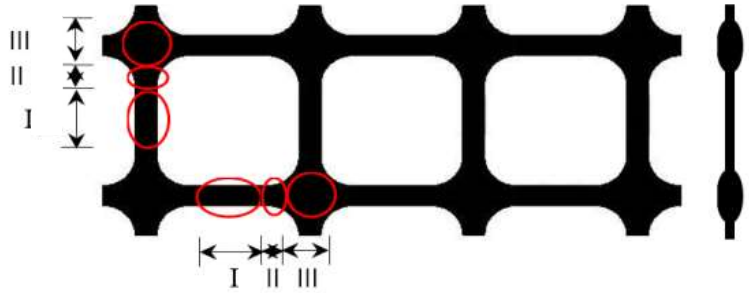

Figure 1. Molecular state partition of biaxially stretched plastic geogrid

ISSN: 2414-1895 DOI: 10.6919/ICJE.202401_10(1).0005

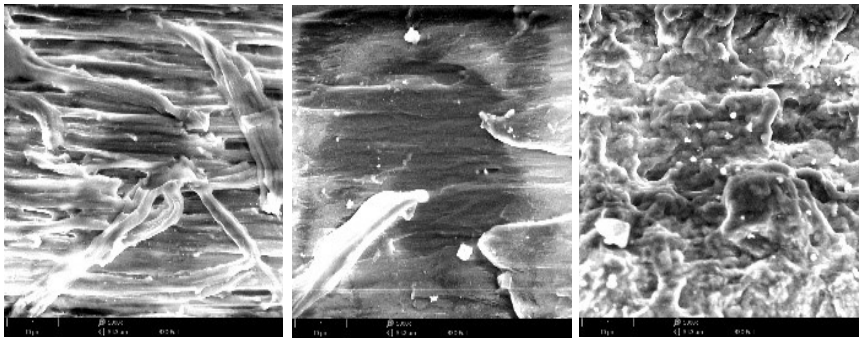

Figure 2. SEN images of the molecular state partition of biaxially stretched plastic geogrid

3. Test Apparatus, Materials and Program

3.1 Test Apparatus

Fig 3 shows a sketch of the tensile test apparatus used in this study. It includes the geogrid clamping device, tensile extension rate device, instrumentation and data acquisition system. There are four grips, two fixed grips and two movable grips. The fixed grips are used to provide side restraint to simulate the limiting effect in the length direction. Both moveable grips are connected to the shaft of motors that determine the tensile extension rate through a rod. There are links from transducers and load cells to the data acquisition system to record the load and strain.

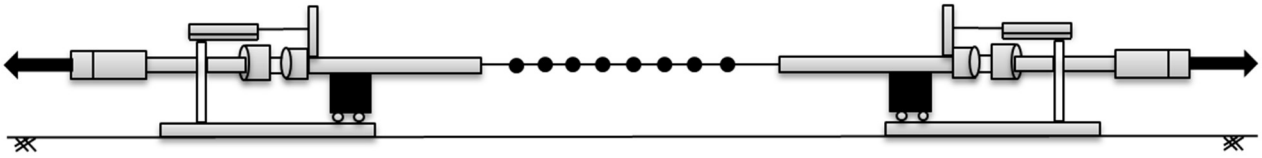

a) Cross-sectional view

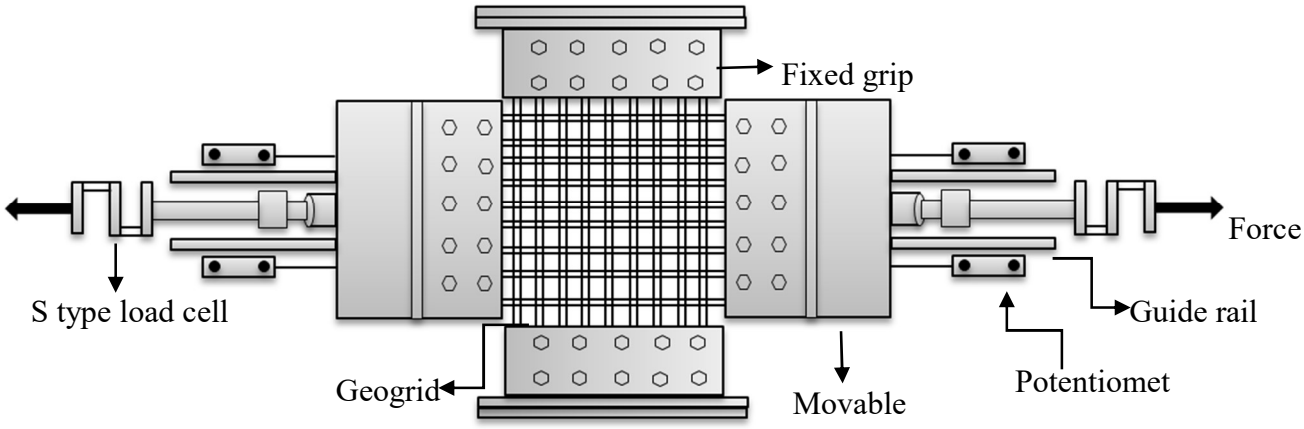

b) Top view

Figure 3. The tensile test apparatus

3.2 Test Materials

The mechanical properties of the PP geogrids used in this paper are listed in Table 1 [14].

Two types of biaxial plastic geogrid with different strengths were tested. The grids were made of polypropylene (PP) and contained 26 ribs per meter on average.

ISSN: 2414-1895 DOI: 10.6919/ICJE.202401_10(1).0005

Table 1. The mechanical properties of the PP geogrids

Geogrid type	Mesh size /cm^2	2% strain tensile stress/(kN•m^{-1})	5% strain tensile stress/(kN•m^{-1})	Ultimate tensile strength/(kN•m^{-1})
TGSG20	14.44	≥8.9	≥15.9	21.7
TGSG40	14.44	≥18.2	≥34.7	42.3

3.3 Test Program

There were two types of geogrid specimen (Fig 4a, Fig4b) with dimensions of 300 mm (length, L) and 300 mm (width, W) outside of the grips. Based on the geogrid installation method at an engineering site, they were stretched in the direction of machine production of the geogrid. Four tensile extension rates of 0.05, 0.1, 1 and 10 mm/min were selected for the tensile tests. The tests ended when the geogrid fractured. The tensile test programs are listed in Table 2.

(a) The geogrid specimen without side restraint (b) The geogrid specimen with side restraint

Figure 4. Two types of geogrid specimen

Table 2. The tensile test program

Type of Geogrid	Side restraint	Tensile rate/ mm•min^{-1}
TGSG20	no	0.05; 0.1; 1; 10
	yes	
TGSG40	no	0.05; 0.1; 1; 10
	yes	

4. Tensile Tests Results and Analysis

The variation of tensile load with strain and the variation of secant tensile stiffness with strain were plotted for all tensile tests performed in the present study. Secant tensile stiffness, $E\varepsilon$, of geogrid (in kN/m) at a given value of strain was calculated by the following equation:

$$E_\varepsilon = \frac{P_\varepsilon}{\varepsilon} \quad (1)$$

where $E\varepsilon$ corresponds to the value of tensile load at strain ε (%).

In order to compare the secant tensile stiffness of a geogrid under side restraint and without side restraint conditions, a secant stiffness improvement factor was defined by:

$$J_{E_\varepsilon} = \frac{(E_\varepsilon)_{sl}}{(E_\varepsilon)_{usl}} \quad (2)$$

ISSN: 2414-1895 DOI: 10.6919/ICJE.202401_10(1).0005

where J_{E_ε} is a secant stiffness improvement factor, $(E_\varepsilon)_{sl}$ is the value of secant tensile stiffness of the geogrid tested under side restraint conditions and $(E_\varepsilon)_{usl}$ is the value of secant tensile stiffness of geogrid tested without side restraint.

4.1 Tensile Properties of Geogrids

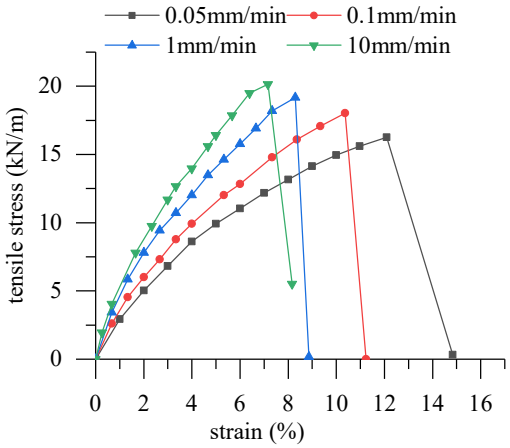

(a) TGSG20 tensile stress-strain curve without side restraint

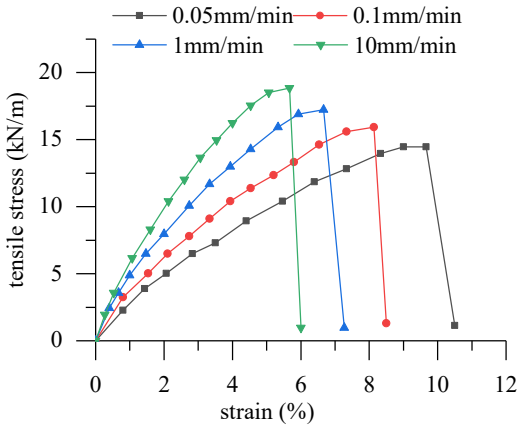

(b) TGSG20 tensile stress-strain curve with side restraint

Figure 5. Tensile stress-strain curves

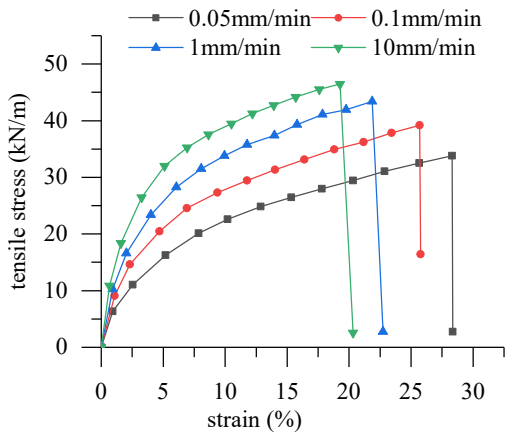

(a) TGSG40 tensile stress-strain curve without side restraint

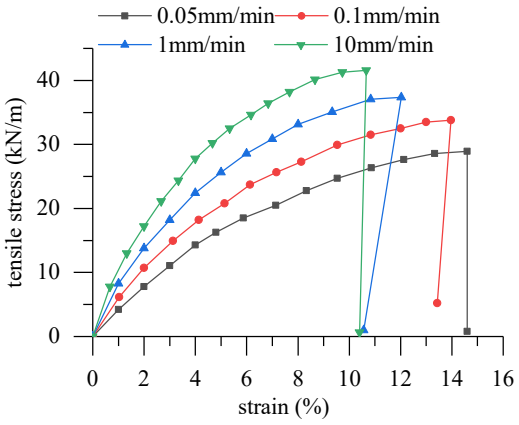

(b) TGSG40 tensile stress-strain curve with side restraint

Figure 6. Tensile stress-strain curves

Figure 5 and Figure 6 show the tensile test result of geogrids under side restraint conditions and without side restraint.

It can be concluded from Fig 5 and Fig 6 that the form of the tensile curves is nonlinear. Tensile extension rate and side restraint do not change the shape of the tensile curve. With increase of extension rate, the tensile strength of geogrid increases, while the strain at fracture decreases. The tensile yield strength and peak strain under the two conditions are listed in Table 3 and Table 4.

ISSN: 2414-1895 DOI: 10.6919/ICJE.202401_10(1).0005

Table 3. The tensile yield strength and peak strain with and without side restraint of TGSG20 geogrid

Property \ Extension rate	0.05	0.1	1	10
tensile yield strength	16.25	18.038	19.175	20.15
	14.463[a]	15.925[a]	17.225[a]	18.85[a]
D-Value	1.787	2.113	1.95	1.3
peak strain	12.81	10.37	8.3	7.17
	9.67[a]	8.13[a]	6.67[a]	5.67[a]
D-Value	3.14	2.24	1.63	1.5

[a] side restraint

Table 4. The tensile yield strength and peak strain with and without side restraint of TGSG40 geogrid

Property \ Extension rate	0.05	0.1	1	10
tensile yield strength	32.746	37.867	41.894	44.608
	28.925[a]	33.8[a]	37.375[a]	41.6[a]
D-Value	3.821	4.067	4.519	3.008
peak strain	28.3	25.7	21.87	19.27
	15.6[a]	13.97[a]	12.03[a]	10.67[a]
D-Value	12.7	11.73	9.84	8.6

[a] side restraint

It can be noted from Table 3 and table 4 that the existence of side restraint leads to reductions of tensile yield strength and peak strain. The differences in tensile yield strength between with and without side restraint are little affected by tensile extension rate. With increase of tensile extension rate, the peak strain difference between with and without side restraint decreased gradually. Lower values of peak strain of geogrids with side restraint is due to the presence of a side restraint increasing the transverse modulus of rib fibers, which leads to the increase of shear force on adjacent fibers in the relative movement in tension.

For the TGSG20 geogrid, tensile yield strength differences of 1.787kN/m, 2.113kN/m, 1.95kN/m and 1.3kN/m and peak strain differences of 3.14%, 2.24%, 1.63% and 1.5% were found at 0.05mm/min, 0.1mm/min, 1mm/min and 10mm/min, respectively. For the TGSG40 geogrid, tensile yield strength differences of 3.821kN/m, 4.067kN/m, 4.519kN/m and 3.008kN/m and peak strain differences of 12.7%, 11.73%, 9.84% and 8.6% were found at 0.05mm/min, 0.1mm/min, 1mm/min and 10mm/min, respectively.

ISSN: 2414-1895 DOI: 10.6919/ICJE.202401_10(1).0005

4.2 Secant Modulus Characteristics of Geogrids

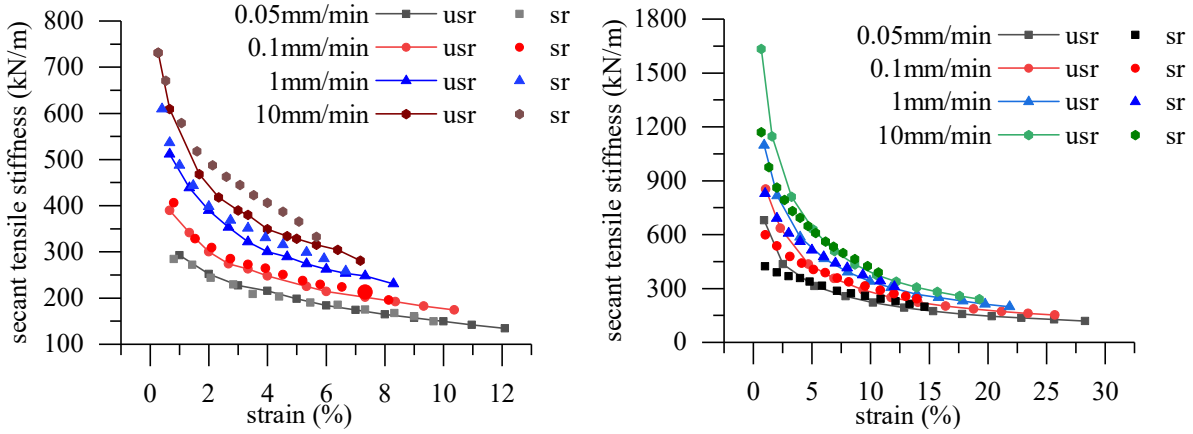

(a)TGSG20 secant tensile stiffness-strain curves (b)TGSG40 secant tensile stiffness-strain curves

Figure 7. Secant tensile stiffness-strain curves

Table 5. Summary of side restraint tensile test results

	Tensile extension rate	$(E_{\varepsilon 0.02})_{usl}$	$(E_{\varepsilon 0.05})_{usl}$	$(E_{\varepsilon 0.1})_{usl}$	$(E_{\varepsilon 0.02})_{sl}$	$(E_{\varepsilon 0.05})_{sl}$	$(E_{\varepsilon 0.1})_{sl}$	$J_{E_{\varepsilon 0.02}}$	$J_{E_{\varepsilon 0.05}}$	$J_{E_{\varepsilon 0.1}}$
TGSG 20	0.05mm/min	251.88	198.25	149.50	246.73	195.88	-	0.98	0.99	-
	0.1mm/min	300.63	231.04	177.12	312.87	241.52	-	1.04	1.05	-
	1mm/min	390.00	281.61	-	398.13	305.61	-	1.02	1.09	-
	10mm/min	442.90	328.25	-	495.10	368.29	-	1.12	1.12	-
TGSG 40	0.05mm/min	517.13	321.66	224.40	390.00	334.26	253.19	0.75	1.04	1.13
	0.1mm/min	688.72	424.66	280.49	536.25	409.87	305.50	0.78	0.97	1.09
	1mm/min	823.63	527.38	338.92	690.63	513.50	360.93	0.84	0.97	1.06
	10mm/min	1066.74	637.60	391.61	861.25	628.51	414.31	0.81	0.99	1.06

It can be noted from Fig 7 that the side restraint has a different effect on different types of geogrid. Fig 7(a) shows that the values of secant tensile stiffness of TGSG20 geogrid when tested under side restraint conditions are higher than when tested under without side restraint conditions. However, for the TGSG40 geogrid, the values of secant tensile stiffness when tested under side restraint conditions are lower than when tested under without side restraint conditions in the early stage of stretching. At the end stage of stretching, the values of secant tensile stiffness when tested under side restraint conditions are higher than when tested under without side restraint conditions (Fig 7(b)).

Improvement in secant tensile stiffness of the geogrid due to side restraint is represented by a secant stiffness improvement factor, J_{E_ε}. For the TGSG20 geogrid, secant stiffness improvement factors of 0.98(0.99), 1.04(1.05), 1.02(1.09) and 1.12(1.12) at 2% (5%) strain were obtained when the geogrid was confined with extension rates of 0.05mm/min,0.1mm/min, 1mm/min and 10mm/min. (Table 5). For the TGSG40 geogrid, secant stiffness improvement factors of 0.75(1.04), 0.78(0.97), 0.84(0.97) and 0.81(0.99) at 2% (5%) strain were obtained when the geogrid was confined with extension rates of 0.05mm/min,0.1mm/min, 1mm/min and 10mm/min. (Table 5). Secant stiffness improvement factors of 1.13 (v=0.1mm/min), 1.09 (v=0.1mm/min), 1.06 (v=1mm/min) and 1.06 (v=10mm/min) was obtained at 10% strain (Table 5). The secant stiffness improvement factors of geogrid at 5% were observed to be close to 1 at the four different extension rates.

ISSN: 2414-1895 DOI: 10.6919/ICJE.202401_10(1).0005

4.3 Failure Mode Analysis of Geogrid

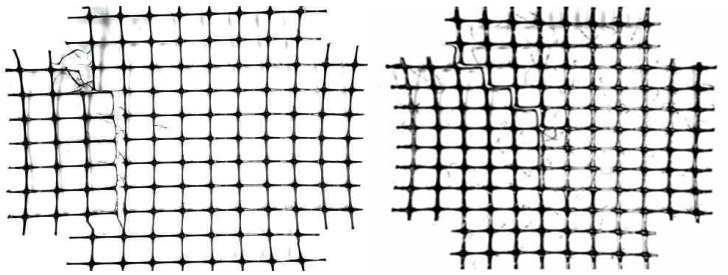

(a) 0.05mm/min (b) 10mm/min

Figure 8. With side restraint tensile failure diagrams

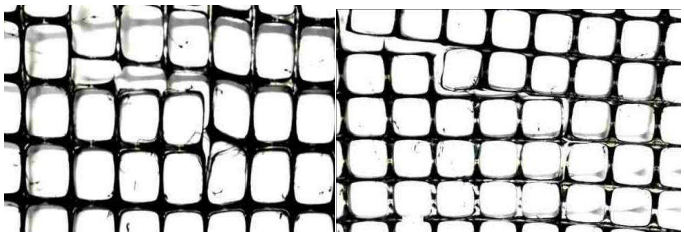

(a) 0.05mm/min (b) 10mm/min

Figure 9. Without side restraint tensile failure diagrams

Figure 8 and Figure 9 show that the failure of geogrid is mainly tearing along the node and rib. However, there were some differences between higher and lower tensile extension rates. At 10mm/min, multiple joints were destroyed first, then the fracture surface passed through the destroyed joints and, finally, the geogrid was torn in brittle fracture. At 0.05mm/min, a few joints failed through the connecting part between rib and node along the rib and, finally, the geogrid was torn in ductile fracture.

5. Conclusion

The effects of side restraint and tensile extension rate on the tensile load-strain characteristics of geogrids were investigated. Secant stiffness improvement factors were determined to quantify the improvement in tensile load-strain characteristics of geogrids with side restraint, compared to without side restraint.

Based on the results presented, the following conclusions can be drawn:

The differences in tensile yield strength between with and without side restraint are little affected by tensile extension rate. With increase of extension rate, the differences in peak strain between with and without side restraint decreased. Lower values of peak strain of geogrids under side restraint are due to the presence of side restraint causing the transverse modulus of the rib fibers to increase, which leads to an increase of shear force on adjacent fibers in the relative movement in tension.

In comparison to without side restraint values, 5% secant tensile stiffness of geogrids TGSG20 and (TGSG40) with side restraint increased by 0.99(1.04) times, 1.05(0.97) times, 1.09(0.97) times and 1.22(0.99) times at extension rates of 0.05mm/min, 0.1mm/min, 1mm/min and 10mm/min, respectively. The secant stiffness improvement factors of geogrid at 5% were observed to be close to 1 at the four different tensile extension rates.

The different tensile extension rates have different effects on the failure mode. At 10mm/min, multiple joints were destroyed first, then the fracture surface passed through the destroyed joints and, finally, the geogrid was torn in brittle fracture. At 0.05mm/min, a few failure joints failed through the connecting part between rib and node along the rib and, finally, the geogrid was torn in ductile fracture.

ISSN: 2414-1895 DOI: 10.6919/ICJE.202401_10(1).0005

Acknowledgments

This study was supported by the National Natural Science Foundation of China (Grant no. 52079078), the Natural Science Foundation of Hebei Province (Grant no. E2018210097/E2019208159), Science and Technology Research Projects of Universities in Hebei Province (Grant no. BJ2020045/ QN2018255). All supports are gratefully acknowledged. We thank BROWNHILL HOUSE (www.eleventowns.com/language.html) for its linguistic assistance during the preparation of this manuscript.

References

[1] YANG Guang-qing. Theory and Engineering Application of Geogrid Reinforced Soil Structure. Beijing: China Science Publishing House, 2010.

[2] P.E. Victor Elias, P.E.; Barry R. Christopher, Ph.D., P.E. and Ryan R. Berg, Mechanically Stabilized Earth Walls and Reinforced Soil Slopes Design & Construction Guidelines, 2001.

[3] J.G. Zornberg, N. Sitar, J.K. Mitchell, Closure to "Performance of Geosynthetic Reinforced Slopes at Failure" by Jorge G. Zornberg, Nicholas Sitar, and James K. Mitchell, J. Geotech. Geoenvironmental Eng. 124 (1998) 670–683. https://doi.org/10.1061/(asce)1090-0241(2000)126:3(285).

[4] M. Ehrlich, B.T. Dantas, J.G. Zornberg, N. Sitar, J.K. Mitchell, Limit Equilibrium as Basis for Design of Geosynthetic Reinforced Slopes, J. Geotech. Geoenvironmental Eng. 8 (1998) 684–698. https://doi.org/ 10.1061/(asce)1090-0241(2000)126:3(286).

[5] WANG Wei, WANG Jian, XUE Jian-hao, XUE Zheng, Analysis of model tests on soft soil subgrade reinforced by geogrid, Rock Soil Mech. 26 (2005) 1885–1891. https://doi.org/10.16285/j.rsm.2005.12.004.

[6] YANG Guang-qing, PANG Wei, LÜ Peng, Experimental study of tensile properties of geogrids, Rock Soil Mech. 29 (2008) 2387–2391. https://doi.org/10.16285/j.rsm.2008.09.028.

[7] R. Hegazy, G.M. Mahmoud, E.H. Hasan, Effect of Strain Rate on Tensile Testing of Geogrid Reinforcements Using Single-Rib and Wide-Rib Specimen, Adv. Polym. Technol. 37 (2018) 1185–1192. https://doi.org/10.1002/adv.21778.

[8] LIN Yu-liang, YANG Guo-lin, Mechanical properties of reinforced soil under tensile load., China Railw. Sci. 30 (2009) 9–13.

[9] M.A. McGown, A., Yogarajah, I., Andrawes, K.Z., Saad, Strain behaviour of polymeric geogrids subjected to sustained and repeated loading in air and in soil, Geosynth. Int. 2 (1995) 341–355.

[10] M.X. Zhang, Q.S. Lin, F.Y. Liu, Tensile experiments of geogrids under cyclic loading, Yantu Lixue/Rock Soil Mech. 31 (2010) 2024–2029. https://doi.org/10.16285/j.rsm.2010.07.037.

[11] Wang, E.L. Xu, B. Zhang, H. Zhong, Z.K. Gao, J.D. Chang, Experimental study on creep properties of plastic geogrid under low temperature, in: Geosynth. Civ. Environ. Eng. - Geosynth. Asia 2008 Proc. 4th Asian Reg. Conf. Geosynth., 2008: pp. 70–73. https://doi.org/10.1007/978-3-540-69313-0_15.

[12] S. Balakrishnan, B.V.S. Viswanadham, Evaluation of tensile load-strain characteristics of geogrids through in-soil tensile tests, Geotext. Geomembranes. 45 (2017) 35–44. https://doi.org/10.1016/ j.geotexmem.2016.07.002.

[13] ASTM. D6637/D6637M, Standard Test Method for Determining Tensile Properties of Geogrids by the Single or multi-rib tensile test, ASTM International, West Conshohocken, PA, USA, 2010. https://doi. org/10.1520/D6637.

[14] ASTM. D4595, Standard Test Method for Tensile Properties of Geotextiles by the Wide-Width Strip Method, ASTM International, West Conshohocken, PA, USA, 2020. https://doi.org/10.1520/D4595-17.Copyright.